ACS Chemical Neuroscience

LETTER

pubs.acs.org/acschemicalneuroscience

Development of a Novel Ligand, [^{11}C]TGN-020, for Aquaporin 4 Positron Emission Tomography Imaging

Yukihiro Nakamura, Yuji Suzuki, Mika Tsujita, Vincent J. Huber, Kenichi Yamada, and Tsutomu Nakada*

Center for Integrated Human Brain Science, Brain Research Institute, University of Niigata, 1 Asahimachi, Niigata 951-8585, Japan

Supporting Information

ABSTRACT: Aquaporin 4 (AQP4), the most abundant isozyme of the water specific membrane transporter aquaporin family, has now been implicated to play a significant role in the pathogenesis of various disease processes of the nervous system from epilepsy to Alzheimer's disease. Considering its clinical relevance, it is highly desirable to develop a noninvasive method for the quantitative analysis of AQP distribution in humans under clinical settings. Currently, the method of choice for such diagnostic examinations continues to be positron emission tomography (PET). Here, we report the successful development of a PET ligand for AQP4 imaging based on TGN-020, a potent AQP4 inhibitor developed previously in our laboratory. Utilizing [^{11}C]-TGN-020, PET images were successfully generated in wild type and AQP4 null mice, providing a basis for future evaluation regarding its suitability for clinical studies.

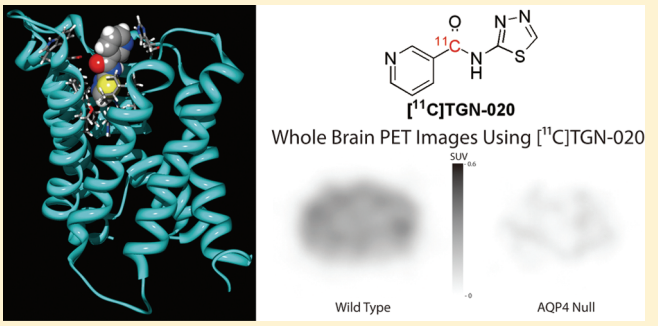

KEYWORDS: Aquaporin 4, positron emission tomography, ^{11}C, TGN-020

The membrane integral water channel Aquaporin 4 (AQP4) has been the subject of much research interest,[1−9] and was found to have a highly restricted distribution in the central nervous system (CNS) along the subpial and perivascular endfeet of glial astrocytes.[2,3] AQP4 has been implicated to play a significant role in the genesis of various neurological disorders, including cerebral edema, epilepsy, and neuromyelitis optica.[4−9] It is, therefore, desirable to develop a noninvasive imaging method for the quantitative visualization of AQP4 distribution in the brain utilizing positron emission tomography (PET).

There have been several reports of small molecules which showed appropriate affinity for AQP4 suitable for development as a radio labeled ligand.[10−18] One such compound is 2-nicotinamido-1,3,4-thiadiazole (TGN-020), which was found to inhibit AQP4 in vitro with an IC_{50} = 3 μM.[16] Its biological effect has, furthermore, been confirmed in live animals.[19] Accordingly, we developed a synthetic method of placing a ^{11}C radio label at the nicotinoyl carbonyl position of the compound to test its suitability as PET ligand.

The synthesis of unlabeled TGN-020 involved the direct condensation of nicotinoyl chloride and 2-amino-1,3,4-thiadiazole, typically in >85% yield of the desired product. The solubility of the resulting compound was generally poor in most solvents, and it was more convenient to carry on to the sodium salt, which has very good aqueous solubility. A similar strategy could then be envisioned for the synthesis of the radio labeled substrate.

Radiosynthesis of [^{11}C]TGN-020 was conducted using a TRACERlab FX_C Versatile automated synthesizer (GE Healthcare). The [^{11}C]-label was introduced into the nicotinic acid moiety by trapping in situ 3-lithiopyridine with [^{11}C]CO_2 as described previously.[20,21] Subsequently, [^{11}C]nicotinic acid was coupled with 2-amino-1,3-thiadiazole to give the target compound (Scheme 1). [^{11}C]TGN-020 was isolated from the crude reaction mixture by semipreparative HPLC. Chemical and radiochemical purity of the samples used for the imaging studies were >95%, as determined by analytical HPLC. Compound identity was confirmed by comparison to an authentic TGN-020 sample.

PET images of [^{11}C]TGN-020 were generated in wild type (WT) and AQP4 null (KO) animals utilizing an eXplore VISTA single-ring PET scanner (GE Healthcare). The detailed description of generating the AQP4 null mouse has been reported previously.[19] A 8−15 MBq aliquot of the purified tracer dissolved in approximately 0.2 mL of vehicle was injected into the tail vein of 8−12 week old mice (average weight 22.9 and 23.4 g for WT and KO animals, respectively). Representative PET images for the WT and KO mice, averaged from 5 to 10 min post injection, are shown in Figure 1.

Overall low uptake of the radio-ligand in the KO mice is likely to reflect lack of AQP4 in skin and muscle, which is known to have a selective distribution of AQP4.[4] High uptake of ligand in both WT and KO mice within the heart indicated that [^{11}C]TGN-020 has some affinity to aquaporin 1 (AQP1), which is shown to have approximately 60% homology with AQP4.

To analyze brain distribution of ligand by eliminating significant interference from skin and muscles, an ex vivo study was performed. Brains of WT and KO mice were harvested en bloc

Received: June 7, 2011
Accepted: June 27, 2011
Published: June 27, 2011

Scheme 1. Synthesis of [^{11}C]TGN-020[a]

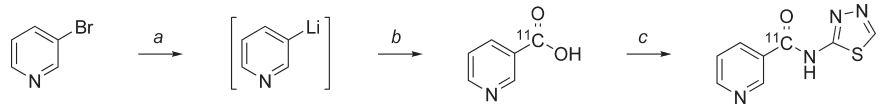

[a] (a) *n*-BuLi, ether, He, −70 °C, 30 min. (b) [^{11}C]CO_2 (g), −70 °C, 3 min. (c) 2-Amino-1,3,4-thiadiazole, EDC·HCl, DMF, 50 °C, 5 min.

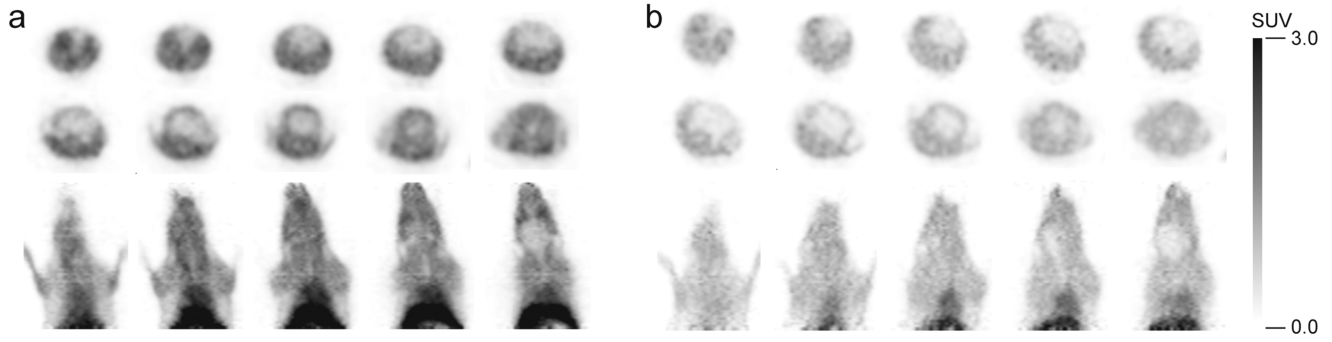

Figure 1. PET images. (a) WT and (b) KO mice.

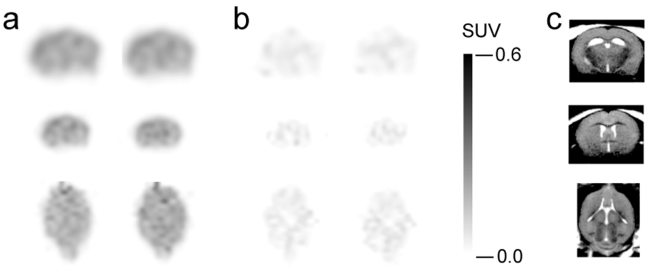

Figure 2. Ex vivo PET images of the brain. (a) WT and (b) KO mouse brains. (c) MRI images of the corresponding brain slices.

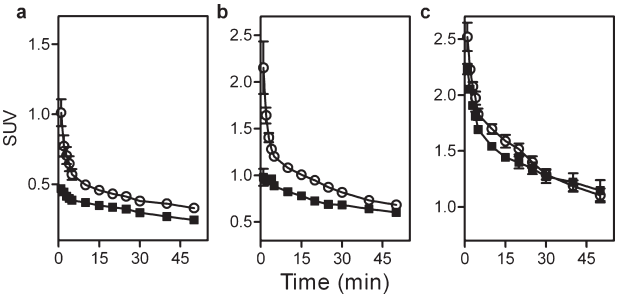

Figure 3. Time course analysis of SUV. Data from WT (n = 6, ○) and KO (n = 4, ■) models are shown along with the standard error of means. (a) Brain, (b) skeletal muscle, and (c) heart.

10 min following the administration of [^{11}C]TGN-020 under identical conditions to the in vivo study. Subsequently, ex vivo PET images were obtained (Figure 2). There is a dramatic difference in ligand uptake within the brain between WT and KO mice. Low but definitely remaining radioactivity within the brain of AQP4 KO mice is believed to reflect uptake of ligand by the tissue with AQP1 such red blood cells.

Time course analyses are shown in Figure 3. Tissues having a significant distribution of AQP4, such as brain (Figure 3a) and skeletal muscle (Figure 3b) also showed a statistically significant higher [^{11}C]TGN-020 uptake in the WT mice compared to those of the KO; P = 0.003 and 0.007, respectively. Conversely, tissues with no significant AQP4 distribution, such as heart (Figure 3c), appeared to have identical ligand uptake in the WT and KO animals (P = 0.2), confirming affinity of [^{11}C]TGN-020 to AQP1. Time course analyses of other tissues are shown in the Supporting Information, along with a table of the corresponding standardized uptake value (SUV) data.

The study confirmed that TGN-020 possesses suitable quality as an AQP4 ligand for human PET imaging studies in spite of its apparent coaffinity to AQP1. In addition to regional specific distribution studies in the brain, quantitative diagnostic studies can be developed for various disease processes, known to have abnormalities in AQP4 distribution such as Duchenne muscular dystrophy, sarcoglycanopathies, or dysferlinopathies.[22,23] In spite of relatively low absolute intensity of radioactivities within the brain of the PET images, considering the specificity of AQP4 distribution, [^{11}C]TGN-020 PET may also be useful for severity analysis of certain disease processes such as neuromyelitis optica, spinal injury, or ocular injuries.[24−28] The slope differences in brain curves between WT and KO mice disappear after the first 15 min presumably due to the first pass extraction, suggesting a high potential of [^{11}C]TGN-020 in ophthalmologic applications. A recent study suggested involvement of AQP4 in activity dependent glial swelling,[29] indicating that [^{11}C]TGN-020 PET may provide hitherto unobtainable quantitative data which may shed light on the molecular basis of the underlying phenomenon used in functional magnetic resonance imaging (fMRI), namely, blood oxygenation level dependent (BOLD) versus signal enhancement by extravascular water protons (SEEP) effects.[30,31]

METHODS

General Synthesis Methods. Reagents of the highest grade available were sourced from Sigma Aldrich (Milwaukee, WI), TCI Chemicals (Tokyo, Japan), or Wako Pure Chemicals (Osaka, Japan)

dx.doi.org/10.1021/cn2000525 |*ACS Chem. Neurosci.* 2011, 2, 568–571

and were used without further purification. Solvents of HPLC grade or higher were additionally sourced from Nacalai Tesuque Chemicals (Tokyo Japan) and were used without further purification. [^{11}C]TGN-020 radiosynthesis was conducted using a TRACERlab FX$_C$ Versatile automated synthesizer (GE Healthcare, Schenectady NY), utilizing a dedicated [^{11}C]CO_2 line. [^{11}C]CO_2 was generated in a PETtrace cyclotron (GE Healthcare) using the ^{14}N(p,α)^{11}C reaction with a 0.5% O_2 + N_2 gas target and was trapped at −100 °C prior to usage. Low temperature control was maintained by direct heating against a liquid nitrogen stream. Isolation of the [^{11}C]-compound was achieved using an integrated semipreparative HPLC system fitted with a microBondapak C18 column (Waters, 7.8 × 300 mm) eluted with 25% ethanol/water plus 0.01% acetic acid. Analytical HPLC was conducted on a Prominence HPLC (Shimadzu, Tokyo, Japan) fitted with a microBondapak C18 column (Waters, 3.9 × 300 mm) eluted with 10% acetonitrile/water plus 0.1% acetic acid. Peak identity was confirmed by comparison against an authentic sample of TGN-020.

[^{11}C]TGN-020 Synthesis. An aliquot of 1.6 M *n*-BuLi (0.1 mL, 0.16 mmol) was added directly to a stirred solution of 3-bromopyridine (0.025 mL, 0.26 mmol) in dry ether (0.5 mL) at −70 °C under He. The resulting solution was stirred at −70 °C for 30 min, at which time [^{11}C]CO_2 (approximately 33.5 GBq) was bubbled through the reaction mixture. Subsequently, dry CO_2 was bubbled through the reaction mixture to ensure the consumption of all organolithium species. The reaction mixture was heated and an aliquot of 1 M HCl (0.3 mL, 0.3 mmol) was added, following which the resulting mixture was evaporated under a dry helium gas stream. A solution of 2-amino-1,3,4-thiadiazole (0.0050 g, 0.050 mmol) and 1-ethyl-3-(3-dimethylaminopropyl)carbodiimide (0.010 g, 0.053 mmol) in dry dimethylformamide (DMF; 0.6 mL) was then added to the residue. The mixture was stirred for 5 min and then evaporated under a stream of dry helium gas. The resulting residue was dissolved in 0.01 M NaOH (0.8 mL) and purified by semipreparative HPLC. The composition of the isolated product was confirmed by analytical HPLC against an authentic TGN-020 standard. [^{11}C]TGN-020 samples used for animal studies had chemical and radiochemical purities of >95%, with radiochemical yields between 150 and 300 MBq.

TGN-020 Reference Synthesis. The synthesis of unlabeled TGN-020 is described in detail in the Supporting Information.

Animal Preparation. All animal experiments were conducted in accordance with the National Institutes of Health guidelines for the care and use of animals in research, and protocols approved by the University of Niigata Animal Care and Use Committee were used. Animals were maintained under standard laboratory conditions including a 12 h light/dark cycle, with food and water available ad libitum. Prior to the study, mice were anesthetized with 1% halothane in 30% oxygen and 70% nitrous oxide administered through a face mask, with the animals breathing spontaneously. Rectal temperature was maintained at 37 ± 0.5 °C using a temperature control unit and heating pad during the anesthesia period. Animals selected for direct brain imaging were deeply anesthetized prior to sacrifice.

Wild-type (WT) and AQP4 (−/−) (KO) C57BL/6 mice were prepared as described previously.[29] Animals used for this study were between 8 and 12 weeks postnatal, with an average 23.4 g weight (WT: 9−12 wk, 22.9 g; KO: 8−12 wk, 23.4 g).

PET Imaging. PET imaging of the WT and AQP4 KO mice was completed using an eXplore VISTA single-ring PET scanner (GE Healthcare, Schenectady NY). [^{11}C]TGN-020 (8−15 MBq, 0.2 mL) was injected via the tail vein. A time-sequential scan was done for 60 min in the list mode with an energy window of 250−700 keV. List-mode data were sorted into 2D sinograms (13 frames: 5 × 1 min, 5 × 5 min, 3 × 10 min), and dynamic 2D images were reconstructed with 2D-OSEM (ordered-subset expectation maximization, 2 iterations and 16 subsets). Decay corrected radioactivity was expressed as a standardized uptake value (SUV). SUV time course data from manually selected areas corresponding to individual tissue types were plotted using GraphPad Prism (version 5.04, GraphPad) for WT (n = 6) and KO (n = 4) animals. Statistical significance was determined for the averaged time-course curves using a single-tail t test.

■ ASSOCIATED CONTENT

Supporting Information. Synthetic details for the reference TGN-020, as well as tissue specific [^{11}C]TGN-020 uptake curves. This material is available free of charge via the Internet at http://pubs.acs.org.

■ AUTHOR INFORMATION

Corresponding Author

*Telephone: +81-25-227-0677. Fax: +81-25-227-0821. E-mail: tnakada@bri.niigata-u.ac.jp. URL: http://coe.bri.niigata-u.ac.jp.

Author Contributions

Y.N. completed the radioligand synthesis, Y.S. was responsible for the PET imaging, M.T. prepared the AQP-KO mice and assisted with animal handling, V.H. synthesized the reference compounds and assisted the development of the radioligand synthesis, K.Y. assisted with the PET imaging, and T.N. conceived and directed the study.

Funding Sources

The work was supported by grants from the Ministry of Education, Culture, Sports, Science, and Technology (Japan) and University of Niigata.

■ ABBREVIATIONS

TGN-020, 2-(nicotinamido)-1,3,4-thiadiazole; AQP4, aquaporin 4; AQP, aquaporin; PET, positron emission tomography; WT, wild-type C57BL/6 mice; KO, homozygous AQP4 −/− C57BL/6 mouse; HPLC, high performance liquid chromatography

■ REFERENCES

(1) Hasegawa, H., Ma, T., Skach, W., Matthay, M. A., and Verkman, A. S. (1994) Molecular cloning of a mercurial-insensitive water channel expressed in selected water-transporting tissues. *J. Biol. Chem. 269*, 5497–5500.

(2) Amiry-Moghaddam, M., and Ottersen, O. P. (2003) The molecular basis of water transport in the brain. *Nat. Rev. Neurosci. 4*, 991–1001.

(3) Venero, J. L., Vizuete, M. L., Machado, A., and Cano, J. (2001) Aquaporins in the central nervous system. *Prog. Neurobiol. 63*, 321–336.

(4) Jung, J. S., Bhat, R. V., Preston, G. M., Guggino, W. B., Baraban, J. M., and Agre, P. (1994) Molecular characterization of an aquaporin cDNA from the brain: Candidate osmoreceptor and regulator of water balance. *Proc. Natl. Acad. Sci. U.S.A. 91*, 13052–13056.

(5) Amiry-Moghaddam, M., Williamson, A., Palomba, M., Eid, T., de Lanerolle, N. C., Nagelhus, E. A., Adams, M. E., Froehner, S. C., Agre, P., and Ottersen, O. P. (2003) Delayed K^+ clearance associated with aquaporin-4 mislocalization: Phenotypic defects in brains of α-syntrophin-null mice. *Proc. Natl. Acad. Sci. U.S.A. 100*, 13615–13620.

(6) Moftakhar, P., Lynch, M. D., Pomakian, J. L., and Vinters, H. V. (2010) Aquaporin expression in the brains of patients with or without cerebral amyloid angiopathy. *J. Neuropathol. Exp. Neurol. 69*, 1201–9.

(7) Lee, T. S., Eid, T., Mane, S., Kim, J. H., Spencer, D. D., Ottersen, O. P., and de Lanerolle, N. C. (2004) Aquaporin-4 is increased in the sclerotic hippocampus in human temporal lobe epilepsy. *Acta Neuropathol. 108*, 493–502.

(8) Hinson, S. R., McKeon, A., and Lennon, V. A. (2010) Neurological autoimmunity targeting aquaporin-4. *Neuroscience 168*, 1009–1018.
(9) Aoki-Yoshino, K., Uchihara, T., Dyuckaerts, C., Nakamura, A., Huaw, J. J., and Wakayama, Y. (2005) Enhanced expression of aquaporin 4 in human brain with inflammatory diseases. *Acta Neuropathol. 110*, 281–288.
(10) Yool, A. J., Brown, E. A., and Flynn, G. A. (2010) Roles for novel pharmacological blockers of aquaporins in the treatment of brain oedema and cancer. *Clin. Exp. Pharmacol. Physiol. 37*, 403–409.
(11) Huber, V. J., and Nakada, T. (2008) Aquaporin-4 as a therapeutic target: a first look. *Drugs Future 33*, 897–909.
(12) Papadopoulos, M. C., and Verkman, A. S. (2008) Potential utility of aquaporin modulators for therapy of brain disorders. In *Progress in Brain Research: Advances in Vasopressin and Oxytocin -- From Genes to Behaviour to Disease* (Neumann, I. D., Landgraf, R., Eds.), Vol. 170, pp 589−601, Elsevier, Oxford.
(13) Wang, F., Feng, X.-C., Li, Y.-M., Yang, H., and Ma, T.-H. (2006) Aquaporins as potential drug targets. *Acta Pharmacol. Sin. 27*, 395–401.
(14) Migliati, E., Meurice, N., DuBois, P., Fang, J. S., Somasekharan, S., Beckett, E., Flynn, G., and Yool, A. J. (2009) Inhibition of Aquaporin-1 and Aquaporin-4 water permeability by a derivative of the loop diuretic bumetanide acting at an internal pore-occluding binding site. *Mol. Pharmacol. 76*, 105–112.
(15) Mola, M. G., Nicchia, G. P., Svelto, M., Spray, D. C., and Frigeri, A. (2009) Automated cell-based assay for screening of aquaporin inhibitors. *Anal. Chem. 81*, 8219–8229.
(16) Huber, V. J., Tsujita, M., and Nakada, T. (2009) Identification of aquaporin 4 inhibitors using in vitro and in silico methods. *Bioorg. Med. Chem. 17*, 411–417.
(17) Huber, V. J., Tsujita, M., Kwee, I. L., and Nakada, T. (2009) Inhibition of aquaporin 4 by antiepileptic drugs. *Bioorg. Med. Chem. 17*, 418–424.
(18) Huber, V. J., Tsujita, M., Yamazaki, M., Sakimura, K., and Nakada, T. (2007) Identification of arylsulfonamides as aquaporin 4 inhibitors. *Bioorg. Med. Chem. Lett. 17*, 1270–1273.
(19) Igarashi, H., Huber, V. J., Tsujita, M., and Nakada, T. (2011) Pretreatment with a novel aquaporin 4 inhibitor, TGN-020, significantly reduces ischemic cerebral edema. *Neurol. Sci. 32*, 113–116.
(20) Murray, A., III, Foreman, W. W., and Langham, W. (1947) The halogen-metal interconversion reaction and its application to the synthesis of nicotinic acid labeled with isotopic carbon. *Science 106*, 277.
(21) Machulla, H.-J., Laufer, P., and Stöcklin, G. (1976) Radioanalytical quality control of ^{11}C, ^{18}F and ^{123}I-labeled compounds and radiopharmaceuticals. *J. Radioanal. Chem. 32*, 381–400.
(22) Wakayama Y. (2010) Aquaporin expression in normal and pathological skeletal muscles: A brief review with focus on AQP4. *J. Biomed. Biotechnol.* published online Jan 17, 2010. DOI: 10.1155/2010/731569.
(23) Au, C. G., Butler, T. L., Egan, J. R., Cooper, S. T., Lo, H. P., Compton, A. G., North, K. N., and Winlaw, D. S. (2008) Changes in skeletal muscle expression of AQP1 and AQP4 in dystrophinopathy and dysferlinopathy patients. *Acta Neuropathol. 116*, 235–246.
(24) Assereto, S., Mastrototaro, M., Stringara, S., Gazzerro, E., Broda, P., Nicchia, G. P., Svelto, M., Bruno, C., Nigro, V., Lisanti, M. P., Frigeri, A., and Minetti, C. (2008) Aquaporin-4 expression is severely reduced in human sarcoglycanopathies and dysferlinopathies. *Cell Cycle 7*, 2199–2207.
(25) Kinoshita, M., Nakatsuji, Y., Kimura, T., Moriya, M., Takata, K., Okuno, T., Kumanogoh, A., Kajiyama, K., Yoshikawa, H., and Sakoda, S. (2009) Neuromyelitis optica: Passive transfer to rats by human immunoglobulin. *Biochem. Biophys. Res. Commun. 386*, 623–627.
(26) Graber, D. J., Levy, M., Kerr, D., and Wade, W. F. (2008) Neuromyelitis optica pathogenesis and aquaporin 4. *J. Neuroinflammation* published online May 29, 2008. DOI: 10.1186/1742-2094-5-22.
(27) Nesic, O., Guest, J. D., Zivadinovic, D., Narayana, P. A., Herrera, J. J., Grill, R. J., Mokkapati, V. U. L., Gelman, B. B., and Lee, J. (2010) Aquaporins in spinal cord injury: The Janus face of aquaporin 4. *Neuroscience 168*, 1019–1035.
(28) Dibas, A., Yang, M.-H., He, S., Bobich, J., and Yorio, T. (2008) Changes in ocular aquaporin-4 (AQP4) expression following retinal injury. *Mol. Vision 14*, 1770–1783.
(29) Kitaura, H., Tsujita, M., Huber, V. J., Kakita, A., Shibuki, K., Sakimura, K., Kwee, I. L., and Nakada, T. (2009) Activity-dependent glial swelling is impaired in aquaporin-4 knockout mice. *Neurosci. Res. 64*, 208–212.
(30) Stroman, P. W., Lee, A .S, Pitchers, K. K, and Andrew, R. D. (2008) Magnetic resonance imaging of neuronal and glial swelling as an indicator of function in cerebral tissue slices. *Magn. Reson. Med. 59*, 700–706.
(31) Figleya, C. R., Leitcha, J. K., and Stromanl, P. W. (2010) In contrast to BOLD: signal enhancement by extravascular water protons as an alternative mechanism of endogenous fMRI signal change. *Magn. Reson. Imaging 28*, 1234–1243.